This is the last draft sent to the Editorial by the authors of the article:

M. GÓMEZ, S. F. MEDINA, P. VALLES
"Determination of Driving and Pinning Forces for Static Recrystallization during Hot Rolling of a Niobium Microalloyed Steel"

ISIJ International
Vol. 45 (2005), Pages: 1711-1720
DOI: 10.2355/isijinternational.45.1711
ISSN: 0915-1559

Determination of Driving and Pinning Forces for Static Recrystallization during Hot Rolling of a Niobium Microalloyed Steel

M. GÓMEZ, S. F. MEDINA, P. VALLES[1]

National Centre for Metallurgical Research (CENIM-CSIC), Av. Gregorio del Amo 8, 28040-Madrid, Spain

E-mail: smedina@cenim.csic.es

[1] National Institute of Aerospace Technology (INTA), Carretera de Ajalvir, km. 4, 28850-Torrejón de Ardoz, Madrid, Spain

The hot rolling process of a low Nb-microalloyed steel under different interpass time conditions is simulated by means of hot torsion tests. Subsequent graphic representation of the Mean Flow Stress (MFS) versus the inverse of the absolute temperature for each pass allows us to know the critical rolling temperatures (T_{nr}, A_{r3}, A_{r1}) and to characterize the progressive strengthening of austenite due to incomplete recrystallization between T_{nr} and A_{r3}, thanks to the measurement of a magnitude called accumulated stress ($\Delta\sigma$). Optical and electron microscopy studies demonstrate that the evolution of the microstructure and the precipitation state –particularly the mean particle size– over the rolling schedule is strongly dependent on the interpass time. A review is made of the expressions that have been proposed to estimate the values of recrystallization driving (F_R) and pinning forces (F_P). Using these expressions and the experimental data from the hot rolling simulations performed, the evolution of F_R and F_P during rolling is studied. A comparative analysis of hypotheses concerning the interaction between precipitates and migrating grain boundaries is achieved and the methods for estimating the volume fraction of precipitates and the dislocation density are assessed. Though the selected criterion significantly influences the values obtained for both forces, it is found that F_P always grows faster than F_R as the rolling temperature drops, which helps to explain the start of inhibition of the static recrystallization of austenite at temperatures below T_{nr}.

KEY WORDS: microalloyed steel, hot rolling, static recrystallization, strain-induced precipitation, driving forces, pinning forces.

1. Introduction

Microalloying elements dissolved in austenite have a considerable effect on grain growth, progress of recrystallization, and phase transformation. However, the main reason for the presence of these elements in microalloyed steels lies in their precipitation, and particularly in the interaction of particles of these elements (Ti, Nb, V) and interstitials (C, N) with austenite grain boundaries in motion. Whereas solutes hinder the advance of grain boundaries by means of a friction effect originated by the difference in their atomic radius compared with iron, precipitates cause a decrease in the effective grain boundary area and thus in the associated surface energy. The latter leads to an obstruction of grain boundary motion or a pinning effect which is much stronger than the solute drag.

In 1948, Zener [1)] proposed that the driving pressure for grain growth due to the curvature of the boundary would be counteracted in particle-containing materials by a pinning pressure exerted by the particles situated at the boundary. Normal grain growth would be completely inhibited when the grain size reached a maximum, given by the critical radius R_c:

$$R_c = \frac{4}{3} \cdot \frac{r}{f} \quad \text{.....(1)}$$

where r is the radius of the pinning second phase particles and f their volume fraction.

This is a major equation because it demonstrated for the first time that a decrease in the size of second phase particles and an increase in their volume fraction lead to grain refinement. This is crucial not only for microalloyed steels but also for aluminum alloys

and many other materials of industrial interest. As proof of the value of Zener's equation, various authors have confirmed, completed or modified this equation for normal grain growth and have extended it to the case of abnormal growth [2]. All these interpretations of Equation (1) can be adapted to a general expression:

$$R_c = K \frac{r}{f^m} \quad \text{.....(2)}$$

where the adimensional constant K and the exponent m depend on the model considered.

The different versions of equation (2) vary Zener's initial hypotheses, which could be inexact, regarding the geometry of the zone of interaction between particle and grain boundary, the particle distribution, the relationship between boundary curvature and grain radius, and the original distribution of sizes [3-8]. Rios [9] broaches the subject using dissipated energy rather than the equilibrium of forces or pressures proposed by Zener.

Many authors have assessed the close relationship between grain size and precipitation state (size, distribution, volume fraction and stability). Stability refers not only to precipitate dissolution, but also to the disproportionate growth of some particles at the expense of others when holding at temperatures below the solubility temperature (coalescence of particles). If this occurs, growth will be abnormal [8] and the critical radius will not be the same for all the material. Therefore, to control the austenite grain size at high temperatures there must be a high proportion of fine particles and the solubility temperature T_s must be high enough, and it is also essential that the particles do not coarsen or coalesce at temperatures below T_s [10]. The quantity of solute in the matrix will exert an important influence on precipitate coarsening and consequently on the capacity of grain growth

inhibition, both for simple additions and for steels with more than one type of microalloying element or precipitate. In the latter case, a complex dependence on time and temperature may be found [11,12].

One of the most interesting aspects of Zener's equation lies in its application to other annealing phenomena occurring in particle-containing materials besides grain growth, especially the static recrystallization of microalloyed steels. Many models on the inhibition of recrystallization by precipitates of microalloying elements have been presented [13,14]. In summary, all of these hypotheses start from the same idea, similar to that of Zener: there is a driving pressure (usually taken as a "force") for recrystallization F_R that comes from the stored energy of the deformation applied to the steel, and an opposite pinning force F_P exerted by the precipitates that lessens the grain boundary surface energy. Depending on the net driving pressure (F_R-F_P), recrystallization progresses or stops. Hansen et al. [13] establish three regions for the progress of recrystallization: if $F_R < F_P$, recrystallization stops completely; if $F_R > F_P$, the austenite grain boundaries can move slowly; if $F_R >> F_P$, the precipitates do not exert a significant effect on grain boundary motion. Nevertheless, most authors [14,15] simplify the matter and postulate that recrystallization will halt when the net force per grain boundary unit area reach values of less than or equal to zero ($F_R \leq F_P$). Palmiere et al. [16] affirm that F_R and F_P are equal at T_{RXN}, a temperature at which recrystallization is practically inexistent. This point must be considerably lower than the no-recrystallization temperature (T_{nr}), since it delimits the beginning of recrystallization inhibition during hot rolling.

Although the problem seems quite simple to pose, the difficulty comes from the correct calculation of F_R and F_P. Some of the factors influencing the values of these forces are

parameters whose determination is not easy and have to be estimated. The different criteria or hypotheses adopted will lead to considerable differences, even of some orders of magnitude.

2. Expressions for the calculation of driving and pinning forces for static recrystallization

2.1. Driving force

According to the model of strain-induced grain boundary motion [17], the driving force for recrystallization F_R comes from the difference in the volume strain energy (i.e. the dislocation density) across the moving boundary separating two adjacent subgrains. This force can be expressed as:

$$F_R = \mu b^2 \Delta\rho / 2 \quad \text{.....(3)}$$

where μ is the shear modulus ($4 \cdot 10^4$ MN/m^2 for austenite), b is the Burgers vector ($2 \cdot 10^{-10}$ m) and $\Delta\rho$ is the change in dislocation density associated with the migration of the recrystallization front into the deformed region. Although equation (3) does not reflect the influence of the temperature, this magnitude is indirectly taken into account through the value of $\Delta\rho$. Due to the lack of direct and reliable measurements, the value of $\Delta\rho$ has to be estimated. To do this, most authors [14,16,18] use the equation proposed by Keh [19], which relates the increase in dislocation density during work hardening $\Delta\rho$ to the rise in flow stress $\Delta\sigma$:

$$\Delta\sigma = 0.2\ \mu\ b\ \sqrt{\Delta\rho} \quad \text{.....(4)}$$

The value of $\Delta\sigma$ must be obtained by subtracting the initial flow stress σ_0 from the maximum or final flow stress σ reached in the σ-ε curve of the deformation step, as shown by Dutta et al. [20]:

$$\Delta\sigma = \sigma - \sigma_0 = M\alpha\,\mu\,b\sqrt{\Delta\rho} \quad \text{.....(5)}$$

where M is the Taylor factor of the studied material and α is a constant taken to be 0.15. However, it is very common to make $\Delta\sigma$ equal to the maximum or applied stress [21], which is especially suitable for the case of stress-strain curves extracted from torsion tests, where the determination of σ_0 is difficult. According to experimental observations in hot torsion tests carried out at 1000 ºC, σ_0 is approximately equal to $\sigma_p/3$ where σ_p is the peak stress. With regard to hot rolling simulations, σ_0 would respectively correspond to 55% and 45% of the maximum stress for pass strains of ε = 0.20 and 0.35. Palmiere et al. [16] affirm that the stress obtained from mechanical testing represents an average flow stress and recommend calculating F_R by considering the flow stress at the grain boundaries, which is approximately 1.5 times the average flow stress. In an earlier paper these authors measured a potential driving force by calculating the area under the flow curve [15].

Although equation (4) is very commonly used, it should be taken into account that Keh's work deals with alpha iron and that the relationship between stress and dislocation density must be different when studying austenite. Equation (5) is more general and can be applied to gamma iron by using M = 3.1 [20]. However, in this case the authors needed to introduce a "fitting factor" [22] to adjust the dislocation density predictions, which again shows the

difficulty of obtaining an accurate estimation of $\Delta\rho$ from $\Delta\sigma$ values. Equation (5) is almost equivalent to that used by Sun et al. [21] where $\alpha = 1/2\pi = 0.159 \approx 0.15$.

2.2. Pinning force

According to Zener [1], the pinning force F_P arises from the area of boundary blanked off by precipitates. The surface area of a precipitate replaces a portion of the grain boundary, so the movement of the boundary beyond the particle will need a supplementary effort to increase the grain boundary area. This effort corresponds to the pinning force F_P exerted by the particles on the boundary in motion. For a population of N_s particles per grain boundary unit area with a mean radius r, F_P will be:

$$F_p = \pi\, r\, \gamma\, N_s \quad \text{.....(6)}$$

where γ is the interfacial energy per grain boundary unit area (0.8 J/m^2 in austenite). This equation was later modified by Gladman [4]:

$$F_p = 4\, r\, \gamma\, N_s \quad \text{.....(7)}$$

Knowing that the number of particles per unit volume N_v and volume fraction f obey:

$$N_v = \frac{3f}{4\pi r^3} \quad \text{.....(8)}$$

three different models to calculate pinning force F_P have been proposed, depending on the N_s-N_v relationship:

a) Rigid boundary model (RBM). This is the simplest and the least realistic model and assumes that a rigid boundary (not deflected by particles) in motion interacts only with those particles of random distribution whose centers lie within $\pm r$ of the boundary plane.

b) Flexible boundary model (FBM) [14]. An infinitely flexible boundary can interact with any particle with a radius r in the three-dimensional array until it is fully pinned. This is an opposite extreme of RBM and yields much higher F_P values.

c) Sub-boundary model (SBM) [13]. This model assumes that particles can exist on subgrain boundaries in the hot-worked structure prior to the start of recrystallization. This model predicts higher F_P values than the other two.

The basic interpretation of the three models is the same: the finer and more abundant the precipitates (and therefore with a lower spacing), the stronger the pinning force F_P. The formulae that respectively express this dependence for the models are:

$$F_p = \frac{6\gamma f}{\pi r} \quad \text{.....(RBM).....} \quad (9)$$

$$F_p = \frac{3\gamma f^{2/3}}{\pi r} \quad \text{.....(FBM).....} \quad (10)$$

$$F_p = \frac{3\gamma f l}{2\pi r^2} \quad \text{.....(SBM).....} \quad (11)$$

l is the average subgrain diameter. Depending on the author, l takes a value of 0.5 μm [13], 0.8 μm [14] or fluctuates between 0.47 and 0.97 μm [23].

With regard to the precipitated volume fraction *f*, this magnitude can be estimated in two completely different ways: by means of thermodynamic calculations [24] or by the application of Ashby and Ebeling's expressions [25] to data from TEM observations.

Precipitate distribution is usually considered to be uniform across the matrix and the grain boundaries. However, it is known that particles preferentially concentrate on defects. Similarly to the comments about stress $\Delta\sigma$ for the calculation of driving force F_R, Palmiere et al. [15,16] postulate that the pinning force must be higher in places close to the boundary than inside the austenite grain, as there are more particles in the former case. These authors confirm in TEM observations that the precipitate volume fraction is 1.5 – 2 times higher at the grain boundaries than inside the grains and calculate two separate pinning forces for grain boundaries and grain interior.

2.3. Estimation of volume fraction *f* by thermodynamic calculations

The volume fraction of precipitates *f* can be determined by establishing a mass balance under equilibrium conditions where the amount of elements (microalloying, interstitials) precipitated at any temperature is predicted by the solubility product. The work of Manohar et al. [24] for titanium nitride (TiN) can be extended to other nitrides of microalloying elements MN (M = Nb, V). To calculate the percentages of dissolved/precipitated microalloying elements and nitrogen it is necessary to consider that the addition of mass percentages of precipitated and dissolved microalloying element (M_p and $[M]_s$ respectively) is equal to the total amount of M (M_{total}), and the same is also valid for nitrogen contents. It is also assumed that the microalloying element and nitrogen react during the precipitation of MN according to their stoichiometric ratio of atomic weights *P* (*e*). If *K* is the solubility product, then:

$$[M]_s + M_p = M_{total} \quad (12)$$

$$[N]_s + N_p = N_{total} \quad (13)$$

$$\frac{M_p}{N_p} = \frac{P(M)}{P(N)} = e \quad (14)$$

$$\log [M]_s [N]_s = \log K = -\frac{A}{T} + B \quad (15)$$

The values of constants A and B depend on the expression chosen to define K [26-38]. The above system of equations can be reduced to a quadratic equation where the precipitated microalloying element (M_p) at a given temperature T is the unknown quantity:

$$M_p{}^2 - e\left(N_{total} + \frac{1}{e} M_{total} \right) M_p + e\left(M_{total} N_{total} - 10^{-\frac{A}{T}+B} \right) = 0 \quad (16)$$

The rest of the mass percentages will be calculated by substituting appropriate values in the above equations. On the other hand, the volume fraction f can be calculated from:

$$f = \frac{V_{MN}}{V_{MN} + V_{Fe}} \quad (17)$$

where V_{MN} is the volume of a mass m_{MN} of precipitated MN and V_{Fe} is the volume of a mass m_{Fe} of austenite. The volume V of a given mass m of a material can be given as:

$$V = m \frac{N_a V_u}{N_u P} \quad (18)$$

where N_a is the Avogadro's number ($6.0222 \cdot 10^{23}$ atoms/mol), V_u is the volume of the unit cell of the material ($(3.59 \cdot 10^{-8})^3$ cm^3 for austenite and the cube of corresponding lattice parameter for MN [39]), N_u is the number of atoms per unit cell of the material (4 for MN and austenite), and P is the atomic weight of the material.

After substituting the values, it follows that:

$$V_{MN} = am_{MN} \quad (19)$$

$$V_{Fe} = 0.125 m_{Fe} \quad (20)$$

the value of the coefficient a is known for each microalloying element (0.19 for TiN, 0.16 for VN and 0.12 for NbN, approximately). On the other hand:

$$m_{MN} = m_M + m_N = m_M + (m_M / e) \quad (21)$$

$$m_{Fe} = 1 - m_{MN} \quad (22)$$

$$m_M = M_p / 100 \quad (23)$$

In this way, the volume fraction of MN precipitates at any temperature can be predicted. The process for any other kind of nitride, a carbide or a carbonitride would be analogous, although stoichiometric ratios e and lattice parameters need to be changed. When decimal exponents appear in the chemical formula and thus in Equation (16), the resolution of the problem will be more complex. Furthermore, it must be known in all cases which compound is the first to precipitate at each temperature (the most stable precipitate), as

changes in the precipitated species during cooling would considerably complicate the calculations.

2.4. Estimation of volume fraction *f* from TEM data

The volume fraction of precipitates can also be estimated in a completely different way, using data obtained in the observation of samples or replicas by means of transmission electron microscopy (TEM). Three data can be extracted from TEM studies: the mean value of measured precipitate diameters (mean particle size *d*), the standard deviation of the size distribution (*s*), and the precipitate number density per observed unit area (N_p). These three values allow the calculation of *f* thanks to the expression presented by Ashby and Ebeling [25] to transform surface measurements from TEM into volume variables. If N_p particles per unit area of replica have been observed, with a mean diameter *d* and a standard deviation *s*, the volume of particles per unit volume of material, called volume fraction *f*, will be:

$$f = \frac{\pi}{6} N_p \left(d^2 + s^2\right) \quad (24)$$

This value can be inserted in Equations (9) to (11) to calculate the pinning force F_P.

Little work has been published comparing the methods and criteria for estimating driving and pinning forces, particularly under testing conditions similar to those of the hot rolling of steel, where supplementary circumstances that complicate the study appear (such as continuous cooling during thermomechanical treatment). The present study attempts to make an overall comparison using Eqs. (3) to (24) and the aforementioned hypotheses.

3. Experimental procedure

The studied steel was manufactured by Electroslag Remelting (ESR) in a laboratory unit capable of producing 30 kg ingots. This technique avoids macrosegregation, both in alloying elements and impurities, and leads to considerably less microsegregation, these defects being present in conventional ingots and continuous casting billets [40]. As **Table 1** shows, this steel has a very low niobium addition (0.007% Nb). Niobium is known to be the microalloying element that most delays static recrystallization kinetics, even when it is in solution. This unusual composition has been chosen to study the influence that low Nb contents can have on inhibition of the static recrystallization of austenite, mainly caused by the grain boundary pinning effect of strain-induced precipitates.

Rolling simulation tests were carried out in a computer-controlled hot torsion machine, on specimens with a gauge length of 50 mm and a diameter of 6 mm. Prior to the simulation tests the specimens were austenitized at a temperature of 1250 ºC for 10 min. These reheating conditions were enough to achieve the complete dissolution of niobium precipitates, as the solubility temperatures calculated for carbonitrides, nitrides and carbides are equal to 1037 ºC, 965 ºC and 986 ºC, respectively [26]. The temperature was then lowered to that corresponding to the first pass, which was 1150 ºC. The simulations consisted of the performance of 20 passes, with a temperature step of 25 ºC between passes, the last pass being carried out at 675 ºC. The strain applied in each pass was 0.35 and the strain rate was equal to 3.63 s^{-1}. To study the influence of the interpass time (Δt) on several aspects (microstructure, precipitation state, pinning forces), two different values of Δt were used (20 and 200 s).

Four samples were water-quenched from the same temperatures (900 ºC and 775 ºC) along the two planned hot rolling simulation schedules. With each sample a last deformation step was performed and the temperature was then lowered 25 ºC for the corresponding interpass time to reach the quenching temperature. Microstructures were observed on a longitudinal surface of the specimens at 2.65 mm from the axis and the characteristics of the precipitates were determined by TEM, using the carbon extraction replica technique. In each replica a population of no less than 467 particles was counted and their size was measured with the aim of calculating the mean size, the standard deviation of their distribution, and the particle number density.

4. Results and discussion

4.1. Hot rolling simulations. Critical temperatures and accumulated stress.

The torsion test gives the values of applied torque versus the number of turns made on the specimen, which are respectively transformed into equivalent stress and strain using Von Mises criterion [41]. **Figure 1** results from this transformation and shows the simulation of 20 rolling passes for the studied steel for an interpass time of 20 s. In the first deformations the stress rises as the temperature decreases, after which there is a change in the slope with a growth in the stress, which means a greater tendency to strengthening. Later, the stress drops and then grows again in the final passes.

Thanks to the method of Jonas et al. [42-46], the Mean Flow Stress (MFS) –which is determined in each step by dividing the area below the stress-strain curve by the applied strain– can be represented against the inverse of the absolute temperature to obtain plots

such as **Figure 2**. In this figure the evolution of the stress values observed in **Figure 1** can be better explained and four zones can successively be distinguished:

I) Complete recrystallization of austenite between passes at the highest temperatures. The increase in stress is due only to the decrease in temperature.

II) Inhibition of recrystallization and supplementary strengthening of austenite, manifested by an increase in the slope.

III) Austenite→ferrite partial transformation. MFS drops as the temperature decreases because ferrite is softer than austenite.

IV) End of ferrite formation followed by eutectoid transformation. The stress rises again because the remaining austenite transforms into pearlite.

The intersection of the straight regression lines of phases I and II defines the value of the no-recrystallization temperature (T_{nr}), which represents the start of inhibition of the static recrystallization of austenite during hot rolling. The intersection of the regression lines of phases II and III determines the value of the phase transformation temperature A_{r3} and the value of A_{r1} is situated at a point close to the minimum of the parabola corresponding to phases III and IV [43]. In this way, the values found for the three critical temperatures when the interpass time was 20 s were: T_{nr} = 924 ºC, A_{r3} = 743 ºC, A_{r1} = 718 ºC. When deformed at temperatures below T_{nr}, austenite accumulates a stress $\Delta\sigma$ which is due to incomplete recrystallization. The value of the accumulated stress $\Delta\sigma$ can be measured from the graph of MFS versus the inverse of the temperature and will be given by the length of the vertical segment limited by the phase I and phase II regression lines [47] as is illustrated in **Figure 2**. When T = A_{r3}, $\Delta\sigma$ reaches its maximum value, which in this case is equal to 26 MPa.

Figure 3 shows the graphic representation of MFS versus the inverse of the absolute temperature for an interpass time of 200 s. In this second case, the longer time between passes leads to a much lower value of T_{nr} (753 ºC), very close to the A_{r3} phase transformation temperature (725 ºC). The maximum accumulated stress value (12 MPa) is also lower than that obtained when the interpass time is 20 s. This small value of $\Delta\sigma$ makes it impossible to discern a drop in the MFS value and to determine the value of A_{r1}.

4.2. Microstructure of quenched samples

Applying the same deformation conditions as in **Figures 2** and **3**, four samples were quenched from 900 and 775 ºC after performing the corresponding number of previous rolling simulation passes. **Figure 4** shows the microstructure observed in these samples, and serves to illustrate the evolution of the austenite microstructure during hot rolling and informs about the influence of interpass time on this evolution.

Figure 4a shows the microstructure of a specimen quenched from 900 ºC after performing 10 passes of a rolling simulation with a pass strain of $\varepsilon = 0.35$ and an interpass time of 20 s (MFS graph in **Figure 2**). Although austenite grain refinement caused by successive deformations makes it difficult to distinguish recrystallized and unrecrystallized grains, it can be seen that, at this temperature, just below T_{nr}, recrystallization is not complete and there are some slightly bigger and elongated unrecrystallized grains. At the end of the austenitic region (775 ºC, **Figure 4b**), the austenite has covered several passes inside the no-recrystallization domain, but there has also been time to reach a certain degree of recrystallization during successive interpass times. Thus the final microstructure consists of a mixture of elongated deformed grains and very fine equiaxial recrystallized grains.

Two other rolling simulation + quenching tests from 900 ºC and 775 ºC were carried out applying the same strain of 0.35 but using a much longer interpass time of 200 s (MFS plot in **Figure 3**). The first corresponds to a temperature well above T_{nr}, where the interpass time is long enough to allow complete recrystallization and coarsening of the recrystallized grains between rolling passes (compare **Figure 4c** to **4a**). The second sample, quenched from 775 ºC (**Figure 4d**), shows some elongated grains, revealing that static recrystallization is incomplete even before T_{nr} (753 ºC) is reached. Nonetheless, comparison of **Figures 4d** and **4b** shows how the reduction in the interpass time is crucial to obtain a hardened austenite at the end of rolling, i.e. to reach a near to pancake structure prior to the phase transformation.

On the other hand, observing **Figures 4b** and **4d** and the respective accumulated stress values, it may be concluded that $\Delta\sigma$ is an adequate estimation of austenite strengthening between T_{nr} and A_{r3}.

4.3. Precipitation state during hot rolling

Austenite strengthening below T_{nr}, manifested by the accumulated stress $\Delta\sigma$ measured on the MFS curve and the elongation of grains observed in the micrographs, is mainly caused by the inhibition of static recrystallization originated by the pinning effect of very fine Nb precipitates on austenite grain boundary motion. The precipitation state of the four quenched samples was studied by TEM, using the extraction replica technique. As can be seen in **Figure 5**, the particles are usually square or rectangular-shaped and have rounded corners. They are often grouped in clusters or lined up, and coalescence can be observed in both fine and coarse particles.

Energy dispersive X-ray analysis spectra of particles observed in the quenched samples (**Figure 6a**) show the existence of Nb and N in the precipitates. As the observed material is a graphite replica, carbon will be always present in the spectra and it will not be possible to discern whether the observed particle is a pure niobium nitride or a carbonitride. On the other hand, electron diffraction patterns (**Figure 6b**) reveal the existence of an f.c.c. structure in all cases, with lattice parameters fluctuating between 0.437 and 0.455 nm. These values could correspond to niobium carbides, nitrides, or generically carbonitrides [39]. Therefore it may be concluded that the particles precipitated during the hot rolling of the studied steel are niobium carbonitrides whose C/N ratio varies slightly.

Particle size is the most remarkable difference in the precipitation state of the samples. After counting and measuring the size of a large population of particles observed in the replicas, grouping them in 4 nm intervals, it is possible to plot frequency diagrams like those presented in **Figure 7**, where differences in particle size distributions can be assessed. The mean size, standard deviation and particle density were calculated (**Table 2**) and it was found that the size evolution of niobium carbonitrides precipitated during the hot rolling of this low Nb-microalloyed steel noticeably depends on the interpass time Δt. When the steel is deformed with an interpass time Δt of 20 s, the particle size remains roughly constant ($\approx$18 nm) throughout the studied temperature interval. However a longer interpass time of 200 s allows a significant reduction in the mean particle size during rolling (from 54 nm at 900 ºC to 16 nm at 775 ºC). It must be understood that the existing particles never shrink: the lower the temperature, the finer the new particles, so the maximum of the distribution and the mean size are progressively shifted to smaller values.

This different evolution of the size of strain-induced precipitates has been explained as a result of the possible occurrence of precipitate-coarsening phenomena [48]. At 900 ºC, precipitates can enter a coarsening regime if the interpass time is long enough (200 s), since their mean size is much coarser than that measured when the interpass time is 20 s. In the latter case it seems that the interpass time has mainly allowed the nucleation and growth of new particles, but is not long enough for coarsening to take place. Conversely, samples quenched from 775 ºC have similar frequency distributions and mean particle sizes regardless of the interpass time, so there must have been some mechanisms in the rolling process that prevented or retarded precipitate coarsening and favored the nucleation of new particles during the interpass time of 200 s.

Firstly, it should be noted that as the temperature drops, so the diffusivity decreases, which increases the possibility of the formation of new precipitates on defects instead of pre-existing particles. This leads to a finer precipitate size distribution. Furthermore, the stress applied during the deformation steps gives rise to an increase in the dislocation density according to equation (5) [20,22]. In the three-dimensional network of dislocations, the density of dislocation nodes N_v, which can be equated to the density of heterogeneous nucleation sites, is given by:

$$N_v = 0.5\rho^{3/2} \quad \text{.....(25)}$$

Hence, the rise in the stress (σ-σ_0) during deformation leads to an increase in the number of available sites for the nucleation of precipitates during the subsequent interpass time. In the rolling process, the temperature drops as successive passes are applied to the steel. As the steel cools it becomes harder, so the stress necessary to deform the austenite reaches

higher values and the nucleation rate of the precipitates grows, leading to a higher precipitate number density, even in the early stages of the interpass time after deformation. According to traditional theories [49,50], precipitate coarsening by Ostwald ripening does not start before the end of the nucleation and growth stages (i.e. curve "C" of the end of precipitation has been reached). However, Dutta et al. [20,22] have shown that coarsening begins at a very early stage of precipitation and leads to a significant decrease in the precipitate number density. During the time after deformation, precipitate coarsening (greatly favored by accelerated solute diffusion through the dislocation network or pipe diffusion) can occur simultaneously with growth. In any case, even though the precipitates quickly enter the growth and coarsening regime, the very high nucleation rate will lead to a smaller precipitate radius [22].

If –as occurs in rolling– after the interpass time and the decrease in temperature a further deformation is applied, the process of hardening and increase in the density of nucleation sites will take place again. During the subsequent interpass time, new particles will nucleate and grow in new dislocation nodes created by the aforementioned process (Eqs. 5, 25). The original dislocation network will be displaced by the deformation applied and the pre-existing particles will not be connected by dislocations, so coarsening by accelerated pipe diffusion can no longer occur in these particles, which will grow slowly by volume diffusion during the interpass time [20].

When the interpass time is 20 s, there is a hardening due to cooling and an additional accumulated stress, but particle refinement cannot be observed. For short interpass times, T_{nr} corresponds to the early stages of precipitation where the particles are numerous but fine (the interpass time is not long enough to allow coarsening), so the inhibition of

recrystallization by induced precipitation is very strong. It is only when the interpass time increases that the precipitates can coarsen, reducing their pinning effect on the austenite grains. The value of T_{nr} will drop to a temperature where the precipitate volume fraction and mean particle size will be more suitable to delay recrystallization. On the other hand, it should not be neglected that -as will be explained later- replicas are less efficient to capture the smallest particles, so this fact could also contribute to some extent to the conservation of mean precipitate size between 900 ºC and 775 ºC for the specimens with $\Delta t = 20$ s.

4.4. Determination of driving and pinning forces for recrystallization during hot rolling

The applied stress values in the σ-ε curve corresponding to the torsion test pass just before quenching allow the calculation of driving forces F_R by means of Eqs. (3) to (5). On the other hand, **Table 3** shows the mass percentages of niobium, nitrogen and carbon in solution and precipitated at the quenching temperatures for the samples studied by TEM, supposing a mass balance in equilibrium and the precipitation of NbN and $NbC_{0.7}N_{0.2}$. The calculations have been carried out according to Equations (12) to (16) [24] and using the solubility product *K* proposed by Turkdogan [26]. Application of Equation (24) [25] to the data shown in **Table 2** and Equations (17) to (23) to the data shown in **Table 3** yielded the volume fraction *f* and consequently the pinning force F_P values obtained by the different methods and hypotheses. In order to estimate *f*, the precipitation of a niobium carbonitride has been considered to calculate the values of the dissolved and precipitated elements as the solubility temperature of $NbC_{0.7}N_{0.2}$ reaches the highest value.

Tables 4 and **5** respectively show the F_R and F_P values obtained at the two studied temperatures (900 ºC and 775 ºC). As the rolling temperature drops, the steel is harder and

the stress σ and dislocation density $\Delta\rho$ grow, so an increase in the driving force F_R can be observed. F_P also rises during hot rolling because the volume fraction f (i.e. the population of microalloying particles capable of impeding grain boundary motion) increases and the mean particle size d is constant or decreases. Depending on the estimation method applied and the initial criteria or hypothesis proposed, considerable variations in F_R and especially in F_P can be observed, but F_P always grows faster than F_R during cooling. Thus, completion of the static recrystallization of austenite during the interpass time is more and more difficult as the temperature is lowered due to the increasing pinning effect of the precipitates and T_{nr} can appear (as occurs in both simulations).

The pinning forces F_P could have been determined by taking into account the population of the finest particles (e.g. those having $d < 20$ nm). Although the mean particle size decreases, the F_P values would be smaller in this case, as the particle density N_p and the volume fraction f also drop.

Some methods or criteria which lead to unsatisfactory values of F_R and F_P can be rejected. T_{nr} marks the beginning of recrystallization inhibition between successive rolling passes, and if it is assumed that this blocking effect occurs when F_R and F_P are similar, the two forces should not be extremely different in the studied cases, where T_{nr} has been determined. As other authors have previously found [18], the volume fraction f calculated by thermodynamic methods (mass balance) is much lower than that estimated by Eq. (24), and the pinning forces calculated with this f do not reach values of the same order of magnitude as the driving forces. Therefore it seems that when aiming to estimate F_P with known equations, Ashby's method is more appropriate for calculating f than thermodynamic calculations. Certainly, the former is more frequently used [13,15,16,18,23,51] than the latter [14].

Ashby and Ebeling [25] consider that the value of f should be less than the real value, as the number of particles captured by the replica is always smaller than the total amount of precipitates on the sample surface. The main drawback is that two replicas do not necessarily have the same particle capture efficiency, so the comparison of results can be complex. On the other hand, Ashby supposes that the efficiency does not depend on the particle size, although it has later been found that the smallest particles –the most effective in grain boundary pinning– (r < 2 nm) are especially difficult to trap in the replica [13]. Consequently, the particle radius r is overestimated and the volume fraction f is underestimated, so the pinning forces determined by Eq. (24) should be taken as conservative values, despite being considerably higher than those obtained by thermodynamic calculations [16,18].

Some authors [13,14] state that SBM is the most realistic and accurate model, as the predicted F_P is rather higher than that obtained with the other models (RBM, FBM) and is usually of the same order as F_R in cases where recrystallization inhibition is observed. For this reason, SBM is quite often applied [13,15,16,23]. Some of these authors only take into account the finest precipitates [13,16], while others equalize the number of particles per grain boundary area (N_s) to the real number density observed in the replica (N_p) [18] or use thermodynamic data [14]. All of these considerations undervalue f and compensate the high value of F_P obtained by SBM. In the present study (and taking into account data from TEM) SBM offers excessively high F_P values compared with F_R, despite having considered a low average subgrain diameter (l = 0.5 μm). In conclusion, FBM and RBM emerge in this study as more appropriate hypotheses than SBM.

On the other hand, it seems that the most appropriate way of estimating the dislocation density for the calculation of F_R is to use Eq. (4) and the criterion of $\Delta\sigma$ = maximum stress (σ max) or MFS (area under the curve divided by the applied strain), as the other methods lead to greater differences between F_R and F_P. The value of σ_0 has also been found in order to subtract it from the applied stress σ as expressed in equation (5), but the resulting F_R values are rather low. It should be emphasized that F_R represents a potential driving force for recrystallization at the start of the interpass time and derived from the increase in the dislocation density during the deformation stage. This potential may be reduced during the interpass time by the recovery process prior to the onset of recrystallization, by recrystallization itself, and also by the nucleation of new strain-induced precipitates on the dislocations.

Figure 8 shows the evolution of F_R and F_P versus the rolling temperature. **Figure 8a** has been plotted with the average values found for F_R and F_P, while **Figure 8b** shows a particular case where F_R and F_P reach very similar values: calculation of F_R using Eq. (4) with $\Delta\sigma$ = applied stress and estimation of F_P by FBM criterion using TEM data to approximate *f*. In both figures the evolution of F_R versus the temperature is similar: at higher temperatures (900 ºC) the applied stress is almost equal for both interpass times and the driving forces F_R are analogous, but at T = 775 ºC F_R is somewhat higher when Δt = 20 s, as the austenite accumulates a strengthening due to the inhibition of recrystallization below T_{nr} and the increase in the dislocation density $\Delta\rho$ is greater.

With regard to pinning forces, at 900 ºC F_P is lower for the longest interpass time (Δt = 200 s) because this time allows considerable particle coarsening compared to Δt = 20 s. This helps to explain why recrystallization is complete and the T_{nr} is lower (T_{nr} = 753 ºC for Δt

= 200 s) and why recrystallized grain coarsening can even appear as previously explained (**Figures 4a** and **4c**), while for Δt = 20 s the inhibition of recrystallization has already begun (T_{nr} = 924 ºC). However, F_P grows much faster versus the temperature drop for the longest interpass time, probably due to a massive precipitation of fine particles, in such a way that at T = 775 ºC the value of F_P for Δt = 200 s is considerably higher than F_P for Δt = 20 s.

Comparison of the pinning and driving force values is carried out taking the values shown in **Figure 8b**. In this case, the evolution of the (F_P-F_R) balance for the longest interpass time (200 s) agrees well with the T_{nr} value. At temperatures well above T_{nr} where recrystallization is complete (900 ºC) it is found that $F_P < F_R$. However, when the temperature is lowered to 775 ºC the values of F_R and F_P are approximately equal, which is in good agreement with the value of T_{nr} which delimits the start of recrystallization inhibition at 753 ºC. Conversely, the relationship between the T_{nr} values and the (F_P-F_R) balance for the shortest interpass time (20 s) is more difficult to explain, as the driving forces reach higher values than the pinning forces at the two studied temperatures, which are however lower than T_{nr}. To explain this it should be remembered that the appearance of T_{nr} not only depends on the pinning effect of strain-induced precipitates on grain boundary motion but also on solute drag and the interpass time in relation with the static recrystallization kinetics of austenite. For this steel it seems that 20 seconds are insufficient to allow complete recrystallization at the testing temperatures, regardless the (F_P-F_R) balance. These results show the difficulty of establishing a definite relationship between the T_{nr} value and the (F_R-F_P) balance and illustrate the need for more complete studies to explain this aspect.

5. Conclusions

1) There are many hypotheses and variables influencing the value of pinning (F_P) and driving forces (F_R) and the variation in their values can be very large, especially in the case of F_P.
2) During hot rolling, F_R and F_P increase as the temperature drops, but F_P grows faster than F_R and for this reason the inhibition of recrystallization appears at temperatures below T_{nr}.
3) To calculate F_R it is advisable to estimate the increase in the dislocation density $\Delta\rho$ using Keh's equation (Eq. (4)), equating the flow stress $\Delta\sigma$ to the applied or maximum stress or the Mean Flow Stress.
4) When aiming to calculate pinning forces F_P, it is more appropriate to estimate the precipitated volume fraction f from TEM data using the equations proposed by Ashby et al. than using thermodynamic calculations (supposition of a mass balance in equilibrium). The latter yield much lower values of F_P than F_R in cases where both forces are expected to be similar.
5) In this study, the sub-boundary model offers excessively high values of F_P and the flexible boundary model (FBM) seems more appropriate.

ACKNOWLEDGEMENTS

The authors would like to thank the I3P Program (CSIC/European Social Fund) for funding Dr. M. Gómez's grant.

REFERENCES

1) C. S. Smith: *Trans. Metall. Soc. AIME*, **175** (1948), 15. (Ref. 24).

2) P. A. Manohar, M. Ferry and T. Chandra: *ISIJ Int.*, **38** (1998), 913.

3) M. Hillert: *Acta Metall.*, **13** (1965), 227.

4) T. Gladman: *Proc. R. Soc. (London)*, **294** (1966), 298.

5) T. Gladman and F.B. Pickering: *J. Iron Steel Inst.*, **205** (1967), 653.

6) M. F. Ashby, J. Harper and J. Lewis: *Trans. Metall. Soc. AIME*, **245** (1969), 413.

7) V. Randle and B. Ralph: *Acta Metall.*, **35** (1986), 891.

8) T. Gladman: *Mater. Sci. Forum*, **94-96** (1992), 113.

9) P. R. Rios: *Acta Metall.*, **35** (1987), 2805.

10) H. Adrian and F.B. Pickering: *Mater. Sci. Technol.*, **7** (1991), 176.

11) H. Weiss, A. Gittins, G. G. Brown and W. J. Mcg. Tegart: *J. Iron Steel Inst.*, **211** (1973), 703.

12) P. Cotterill and P. R. Mould: Recrystallization and Grain Growth in Metals, Surrey Univ. Press, London, (1976).

13) S. S Hansen, J. B. Van der Sande and M. Cohen: *Metall. Trans. A*, **11A** (1980), 387.

14) L. J. Cuddy: Proc. Int. Conf. Thermomechanical Processing of Microalloyed Austenite, ed. By A. J. DeArdo, G. A. Ratz and P. J. Wray, The Metallurgical Society of AIME, Pittsburgh, PA, (1982), 129.

15) E. J. Palmiere, C. I Garcia, and A. J. DeArdo: Processing, Microstructure and Properties of Microalloyed and Other Modern HSLA Steels, Iron and Steel Society of AIME, Warrendale, PA, (1992), 113.

16) E. J. Palmiere, C. I. Garcia and A. J. DeArdo: *Metall. Mater. Trans. A*, **27A** (1996), 951.

17) P. A. Beck and P.R. Sperry: *J. Appl. Phys.*, **25** (1950), 150.

18) O. Kwon and A.J. DeArdo: *Acta Metall.*, **39** (1991), 529.

19) A. S. Keh: Direct Observations of Imperfections in Crystals, ed. by J. B. Newkirk and J. H. Wernick, Wiley-Interscience, New York, (1962), 213.

20) B. Dutta, E. Valdes and C. M. Sellars: *Acta Metall. Mater.*, **40** (1992), 653.

21) W. P. Sun, M. Militzer and J. J. Jonas: *Metall. Trans. A*, **23A** (1992), 3013

22) B. Dutta, E. J. Palmiere and C. M. Sellars: *Acta Mater.*, **49** (2001), 785.

23) W. M. Rainforth, M. P. Black, R. L. Higginson, E. J. Palmiere, C. M. Sellars, I. Prabst, P. Warbichler and F. Hofer: *Acta Mater.*, **50** (2002), 735.

24) P. A. Manohar, D. P. Dunne, T. Chandra and C. R Killmore: *ISIJ Int.*, **36** (1996), 194.

25) M. F. Ashby and R. Ebeling: *Trans. Metall. Soc. AIME*, **236** (1966), 1396.

26) E. T. Turkdogan: *Trans. ISS*, **3** (1989), 61.

27) D. B. Evans and R. D. Pehlke: *Trans. Metall. Soc. AIME*, **233** (1965), 1620.

28) H. Ghino and K. Wada: Thermodynamic Study of the Deoxidation and Precipitation of Carbides and Nitrides, Yahat Technical Report, 251 (1965), 75.

29) K. J. Irvine, F. B. Pickering and T. Gladman: *J. Iron Steel Inst*., **205** (1967), 161.

30) B. Arosson: Steel Strengthening Mechanisms, Symposium Climax Molybdenum, Zurich, (1969), 161.

31) A. Jacquemot and C. Gatellie: Rapport IRSID, PCM RE-395, (1975).

32) K. Narita: *Trans. Iron Steel Inst. Jpn.*, **15** (1975), 145.

33) Y. Desalos and R. Laurent: Rapport IRSID, No. RI-662, (1977).

34) S. Matsuda and N. Okumura: *Trans. Iron Steel Inst. Jpn.*, **18** (1978), 198.

35) Z. Morita and K. Kunisada: *Trans. Iron Steel Inst. Jpn.*, **18** (1978), 648.

36) B. Chamont: Rapport IRSID, No. RI-961, (1984), 2.

37) P. R. Rios: *Mater. Sci. Technol*., **4** (1988), 324.

38) E. J. Palmiere, C. I. Garcia and A. J. DeArdo: *Metall. Trans. A*, **25A** (1994), 277.

39) W. B. Pearson: A Handbook of lattice spacings and structures of metals and alloys, Pergamon Press, (1958).

40) S. F. Medina and A. Cores: *ISIJ Int.*, **33** (1993), 1244.

41) A. Faessel: *Rev. Metall. CIT*, **33** (1976), 875

42) F. Boratto, R. Barbosa, S. Yue and J. J. Jonas: THERMEC-88 Conf. Proc., ed. by I. Tamura, ISIJ, Tokyo, (1988), 383.

43) F. H. Samuel, S. Yue, J. J. Jonas and B. A. Zbinden: *ISIJ Int.*, **29** (1989), 878.

44) A. Najafi-Zadeh, S. Yue and J. J. Jonas: *ISIJ Int.*, **32** (1992), 213.

45) L. Jiang, A. O. Humphreys and J. J. Jonas: *ISIJ Int.*, **44** (2004), 381.

46) P. Uranga, A. I. Fernández, B. López and J. M. Rodríguez-Ibabe: *ISIJ Int.*, **44** (2004), 1416.

47) M. Gómez, O. Hernanz, S. F. Medina and P. Tarín: *Steel Res.*, **73** (2002), 446.

48) M. Gómez, S. F. Medina and P. Valles: 2nd International Conference on Thermomechanical Processing of Steels TMP'2004, Ed. Marcel Lamberigts, Stahl Eisen, Liege, Belgium (2004), 157.

49) I. M. Lifshitz and V. V. Slyosov: *J. Phys. Chem. of Solids*, **19** (1961), 35.

50) C. Wagner: *Z. Elektrochem.*, **65** (1961), 581.

51) C. García-Mateo, B. López and J. M. Rodríguez-Ibabe: *Mater. Sci. Eng.* A, **303A** (2001), 216.

LIST OF TABLE CAPTIONS

Table 1. Chemical composition of the studied steel (mass %).

Table 2. Results of the study of precipitation state by transmission electron microscopy (TEM). Hot rolling simulations by multipass torsion followed by quenching. Mean particle size (d), standard deviation (s) and number of particles per unit area of replica (N_p).

Table 3. Mass % of Nb, N, C in solution and precipitated at quenching temperatures of samples studied by TEM, supposing the precipitation of NbN and $NbC_{0.7}N_{0.2}$ [24,26].

Table 4. Estimation of recrystallization driving force (F_R) at several temperatures. Comparison of results of different equations relating dislocation density ($\Delta\rho$) and the rise in stress during deformation ($\Delta\sigma$) and study of the influence of criteria to define $\Delta\sigma$. Criterion [*1*]: $\Delta\sigma$ = maximum stress (σmax); criterion [*2*]: $\Delta\sigma = 1.5\cdot\sigma$max; criterion [*3*]: $\Delta\sigma$ = MFS; criterion [*4*]: $\sigma_0 = 0.45\sigma$max ($\varepsilon = 0.35$), $\Delta\sigma = 0.55\cdot\sigma$max.

Table 5. Estimation of recrystallization pinning force (F_P) at several temperatures. Comparison of results given by the models of interaction between particles and grain boundaries and influence of the methods to estimate the precipitated volume fraction f. Average subgrain diameter l = 0.5 μm

LIST OF FIGURE CAPTIONS

Fig. 1. Stress-strain curves corresponding to 20 pass torsion sequence.

Fig. 2. Dependence of Mean Flow Stress (MFS) on inverse of absolute temperature, according to given schedule, Δt = 20 s. Determination of critical temperatures and accumulated stress ($\Delta\sigma$).

Fig. 3. Dependence of Mean Flow Stress (MFS) on inverse of absolute temperature, according to given schedule, Δt = 200 s. Determination of critical temperatures and accumulated stress ($\Delta\sigma$).

Fig. 4. Microstructures obtained by hot rolling simulations in the following conditions: pass strain 0.35, pass strain rate 3.63 s^{-1}. **a)** Interpass time = 20 s, quenching at 900 ºC; **b)** Interpass time = 20 s, quenching at 775 ºC; **c)** Interpass time = 200 s, quenching at 900 ºC; **d)** Interpass time = 200 s, quenching at 775 ºC.

Fig. 5. TEM images of carbon replicas showing Nb precipitates obtained by hot rolling simulations in the following conditions: pass strain 0.35, pass strain rate 3.63 s^{-1}. **a)** Interpass time = 20 s, quenching at 900 ºC; **b)** Interpass time = 20 s, quenching at 775 ºC; **c)** Interpass time = 200 s, quenching at 900 ºC; **d)** Interpass time = 200 s, quenching at 775 ºC.

Fig. 6. a) Energy dispersive X-ray analysis spectrum of a precipitate showing the presence of Nb and N. Sample quenched at 775 ºC; ε = 0.35; Interpass time = 200 s; **b)**

Electron diffraction pattern of a Nb particle, [011] zone axis. Sample quenched at 900 ºC; ε = 0.35; Interpass time = 200 s.

Fig. 7. Precipitate size distributions obtained by hot rolling simulations in the following conditions: pass strain 0.35, pass strain rate 3.63 s^{-1}. **a)** Interpass time = 20 s, quenching at 900 ºC; **b)** Interpass time = 20 s, quenching at 775 ºC; **c)** Interpass time = 200 s, quenching at 900 ºC; **d)** Interpass time = 200 s, quenching at 775 ºC.

Fig. 8. Estimation of recrystallization driving (F_R) and pinning forces (F_P) at 900 ºC and 775 ºC for the two studied hot rolling simulation schedules (Δt = 20 s and Δt = 200 s). **a)** Mean values of calculated F_R and F_P. **b)** F_R calculated after estimation of dislocation density with Equation (4) assuming Δσ = applied or maximum stress and F_P calculated following the FBM criterion and using TEM data to estimate the precipitated volume fraction *f*.

Table 1. Chemical composition of the studied steel (mass %).

C	Si	Mn	P	S	Al	Nb	N	O
0.20	0.20	1.0	0.024	0.013	0.006	0.007	0.0056	0.0057

Table 2. Results of the study of precipitation state by transmission electron microscopy (TEM). Hot rolling simulations by multipass torsion followed by quenching. Mean particle size (d), standard deviation (s) and number of particles per unit area of replica (N_p).

Δt (s)	Number of passes	Temperature (ºC)		TEM Data		
		Last pass	Quenching	d (nm)	s (nm)	N_p ($\cdot 10^{13} m^{-2}$)
20	10	925	900	19	17	3.5
	15	800	775	17	22	9.8
200	10	925	900	54	62	0.9
	15	800	775	16	21	17.7

Table 3. Mass % of Nb, N, C in solution and precipitated at quenching temperatures of samples studied by TEM, supposing the precipitation of NbN and $NbC_{0.7}N_{0.2}$ [24,26].

Temp. (ºC)	Type of precipitate	Nb_s	Nb_p	N_s	N_p	C_s	C_p
900	NbN	0.0028	0.0042	0.0050	0.0006	---	---
	$NbC_{0.7}N_{0.2}$	0.0010	0.0060	0.0054	0.0002	0.1995	0.0005
775	NbN	0.0003	0.0067	0.0046	0.0010	---	---
	$NbC_{0.7}N_{0.2}$	0.0001	0.0069	0.0054	0.0002	0.1994	0.0006

Table 4. Estimation of recrystallization driving force (F_R) at several temperatures. Comparison of results of different equations relating dislocation density ($\Delta\rho$) and the rise in stress during deformation ($\Delta\sigma$) and study of the influence of criteria to define $\Delta\sigma$. Criterion [*1*]: $\Delta\sigma$ = maximum stress (σmax); criterion [*2*]: $\Delta\sigma = 1.5\cdot\sigma$max; criterion [*3*]: $\Delta\sigma$ = MFS; criterion [*4*]: $\sigma_0 = 0.45\sigma$max ($\varepsilon = 0.35$), $\Delta\sigma = 0.55\cdot\sigma$max.

Relation $\Delta\sigma$-$\Delta\rho \rightarrow$		$\Delta\sigma = 0.2\ \mu\ b\ \sqrt{\Delta\rho}$						$\Delta\sigma = M\alpha\ \mu\ b\ \sqrt{\Delta\rho}$ $M = 3.1$; $\alpha = 0.15$	
Criterion for $\Delta\sigma \rightarrow$		[*1*] σmax		[*2*] $1.5\cdot\sigma$max		[*3*] MFS		[*1*] σmax	[*4*] $0.55\cdot\sigma$max
Δt (s)	Last pass temp. (ºC)	$\Delta\sigma$ (MPa)	F_R (MN/m^2)	$\Delta\sigma$ (MPa)	F_R (MN/m^2)	$\Delta\sigma$ (MPa)	F_R (MN/m)	F_R (MN/m^2)	
20	925	162	8.20	243	18.45	124	4.78	1.52	0.46
	800	223	15.54	334	34.96	184	10.56	2.87	0.87
200	925	160	7.99	240	17.99	120	4.53	1.48	0.45
	800	215	14.46	323	32.53	168	8.84	2.67	0.81

Table 5. Estimation of recrystallization pinning force (F_P) at several temperatures. Comparison of results given by the models of interaction between particles and grain boundaries and influence of the methods to estimate the precipitated volume fraction *f*.

Average subgrain diameter l = 0.5 μm

Δt (s)	Quenching Temp. (ºC)	$f \cdot 10^{-4}$	$F_p = 4\ r\ \gamma\ N_s$ (MN/m^2)		
		Equilib. / TEM	RBM: $\frac{6\gamma f}{\pi r}$	FBM: $\frac{3\gamma f^{2/3}}{\pi r}$	SBM: $\frac{3\gamma f l}{2\pi r^2}$
20	900	0.65 / 117	0.0106 / 1.92	0.1317 / 4.22	0.1415 / 25.67
	775	0.74 / 409	0.0132 / 7.24	0.1564 / 10.50	0.1903 / 104.78
200	900	0.65 / 301	0.0036 / 1.70	0.0455 / 2.73	0.0169 / 7.86
	775	0.74 / 656	0.0140 / 12.31	0.1660 / 15.27	0.2144 / 189.13

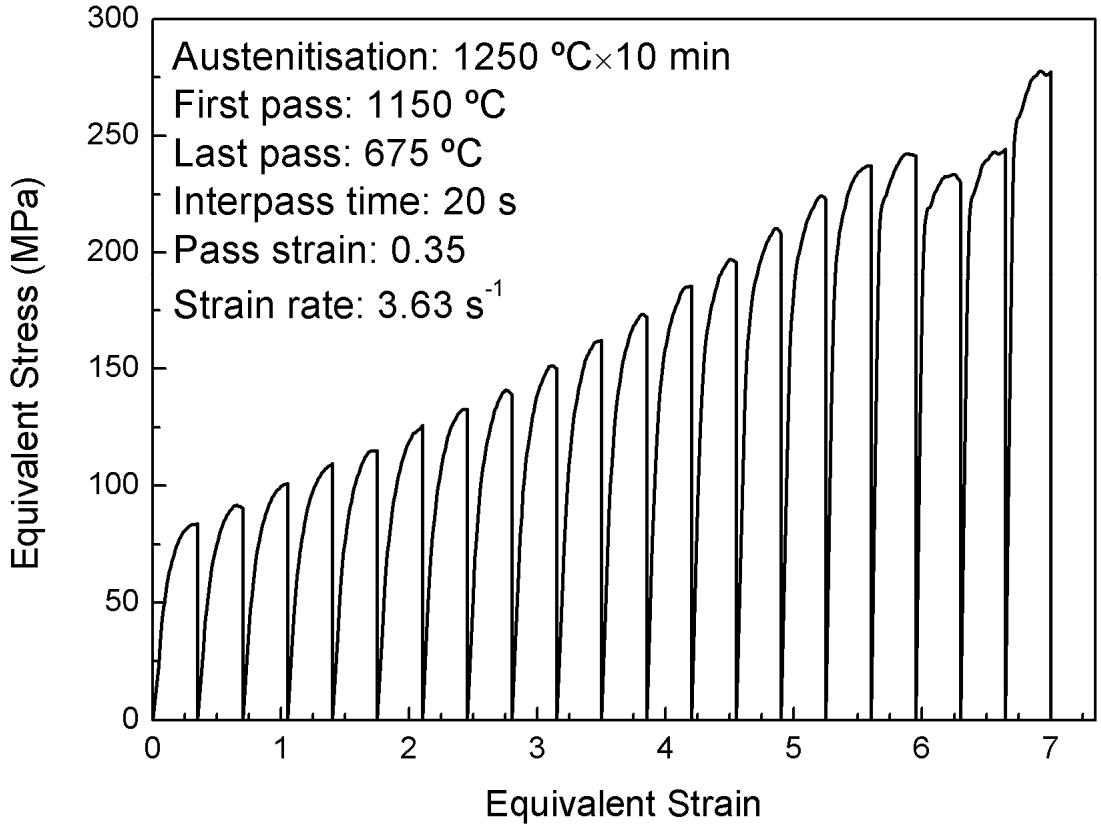

Fig. 1. Stress-strain curves corresponding to 20 pass torsion sequence.

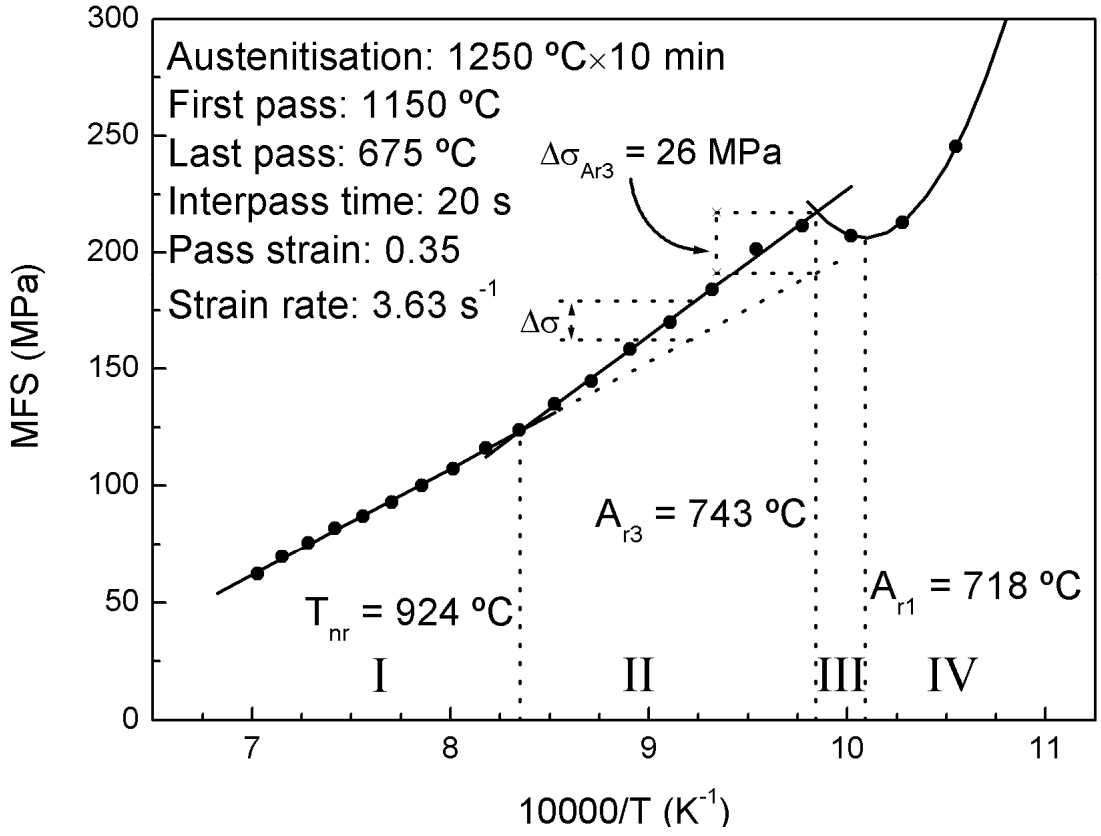

Fig. 2. Dependence of Mean Flow Stress (MFS) on inverse of absolute temperature, according to given schedule, Δt = 20 s. Determination of critical temperatures and accumulated stress ($\Delta\sigma$).

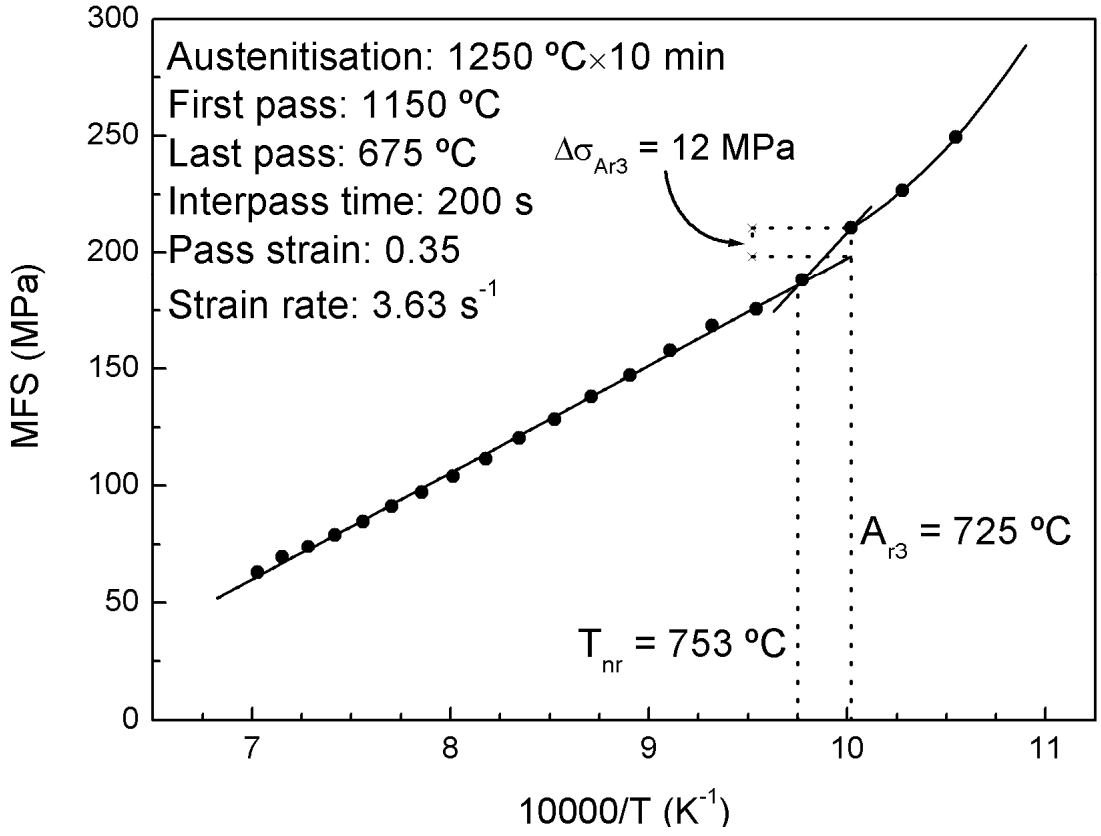

Fig. 3. Dependence of Mean Flow Stress (MFS) on inverse of absolute temperature, according to given schedule, Δt = 200 s. Determination of critical temperatures and accumulated stress ($\Delta\sigma$).

a)

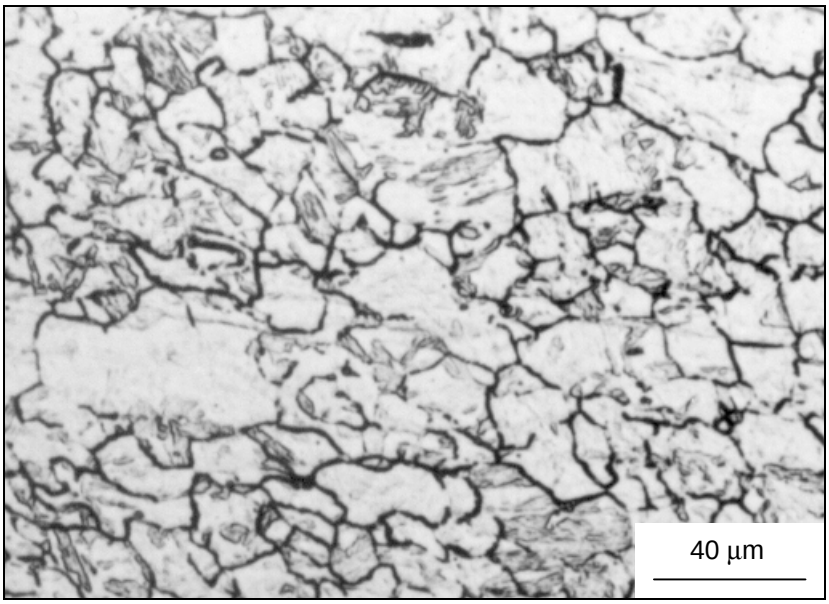

b)

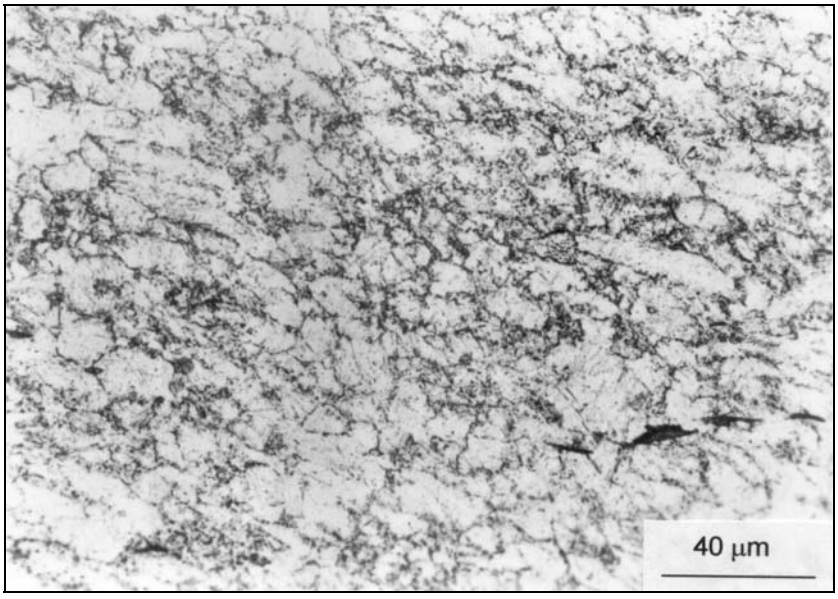

c)

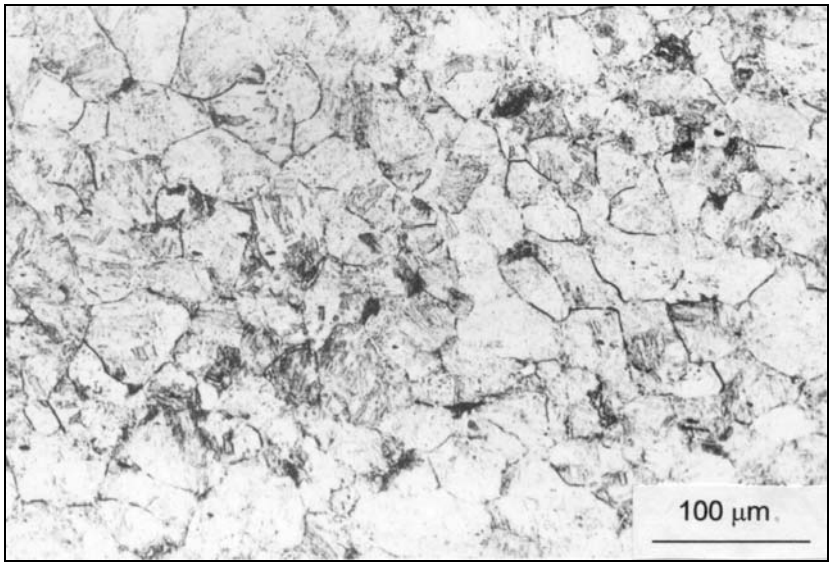

d)

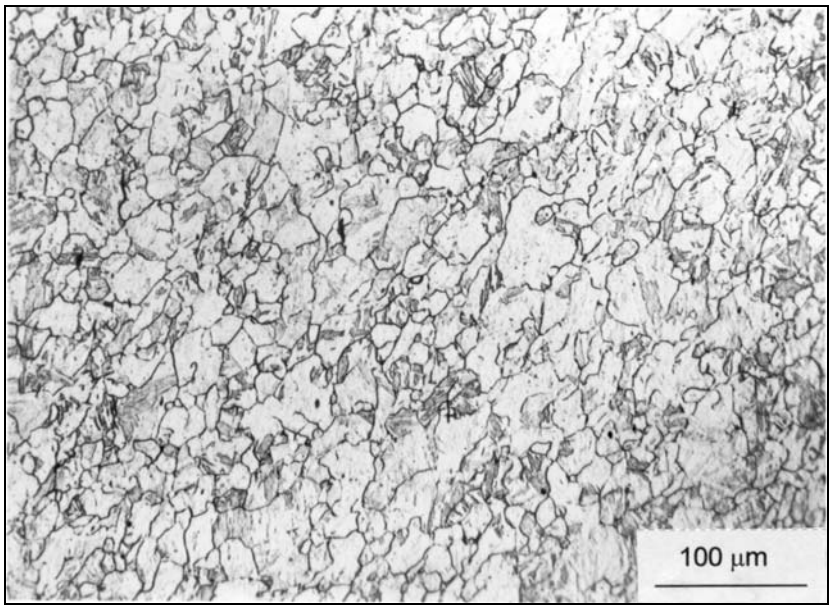

Fig. 4. Microstructures obtained by hot rolling simulations in the following conditions: pass strain 0.35, pass strain rate 3.63 s^{-1}. **a)** Interpass time = 20 s, quenching at 900 ºC; **b)** Interpass time = 20 s, quenching at 775 ºC; **c)** Interpass time = 200 s, quenching at 900 ºC; **d)** Interpass time = 200 s, quenching at 775 ºC.

a)

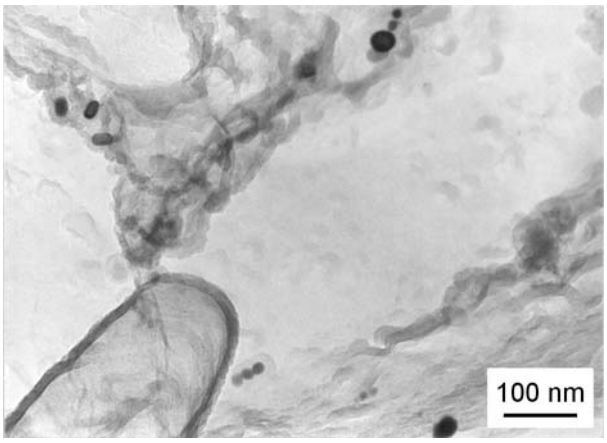

b)

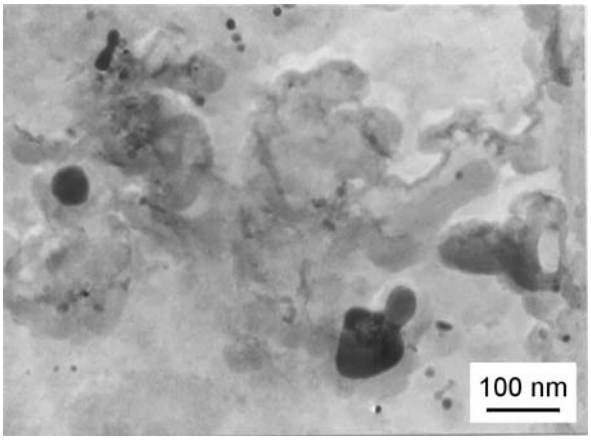

c)

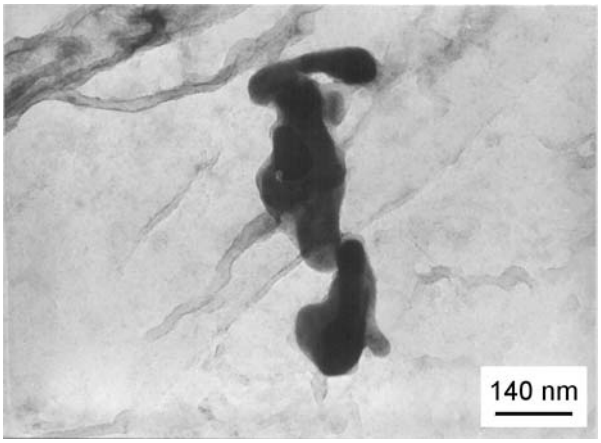

d)

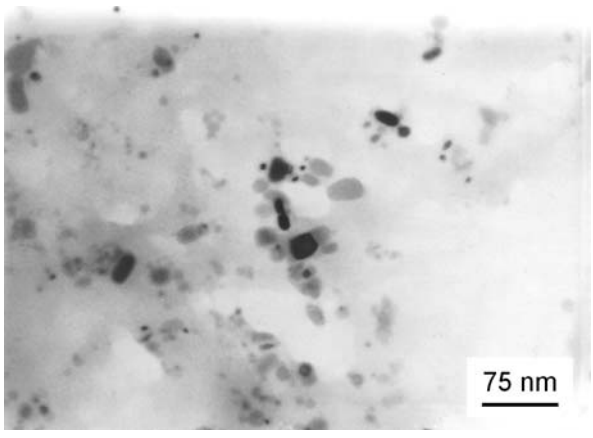

Fig. 5. TEM images of carbon replicas showing Nb precipitates obtained by hot rolling simulations in the following conditions: pass strain 0.35, pass strain rate 3.63 s^{-1}. **a)** Interpass time = 20 s, quenching at 900 ºC; **b)** Interpass time = 20 s, quenching at 775 ºC; **c)** Interpass time = 200 s, quenching at 900 ºC; **d)** Interpass time = 200 s, quenching at 775 ºC.

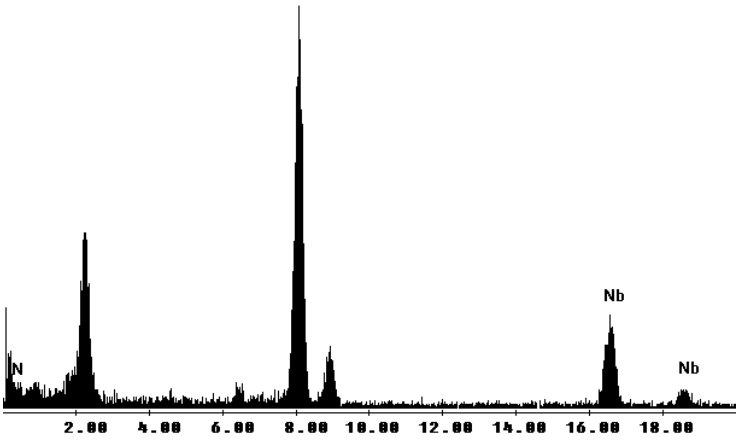

a)

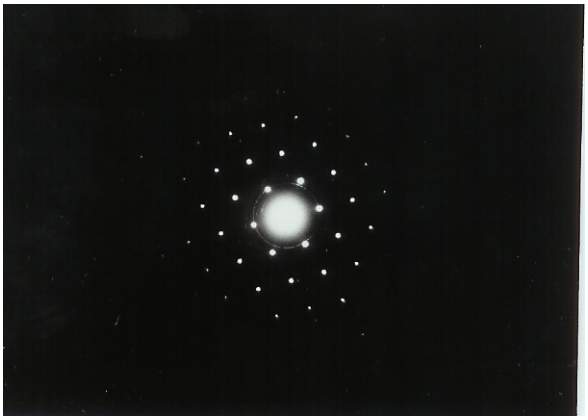

b)

Fig. 6. **a)** Energy dispersive X-ray analysis spectrum of a precipitate showing the presence of Nb and N. Sample quenched at 775 ºC; ε = 0.35; Interpass time = 200 s; **b)** Electron diffraction pattern of a Nb particle, [011] zone axis. Sample quenched at 900 ºC; ε = 0.35; Interpass time = 200 s.

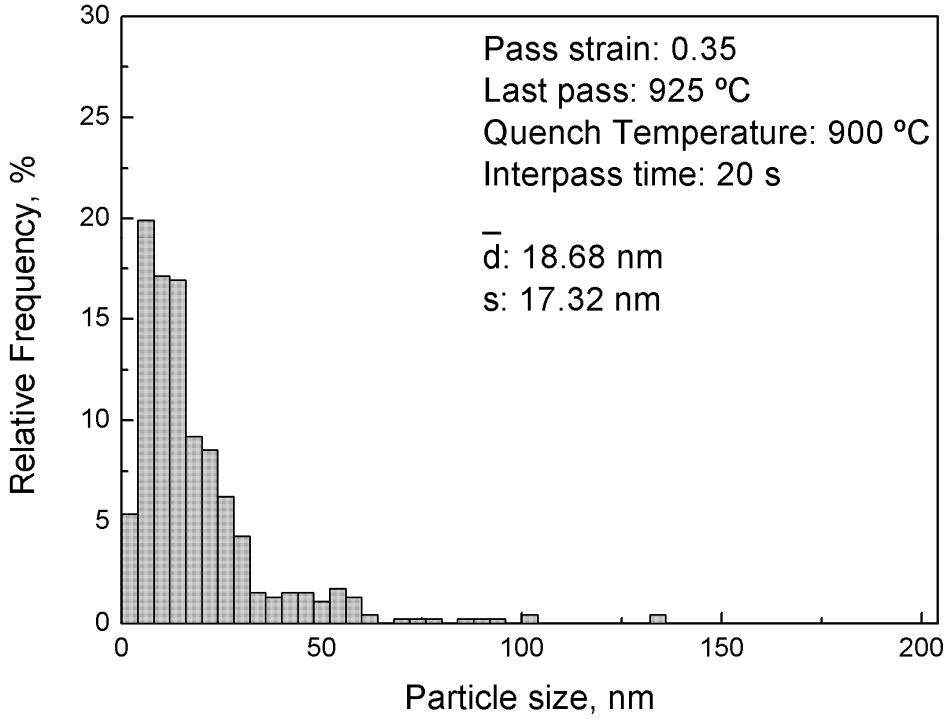
Pass strain: 0.35
Last pass: 925 ºC
Quench Temperature: 900 ºC
Interpass time: 20 s
d: 18.68 nm
s: 17.32 nm
Relative Frequency, %
Particle size, nm
0
5
10
15
20
25
30
0
50
100
150
200

a)

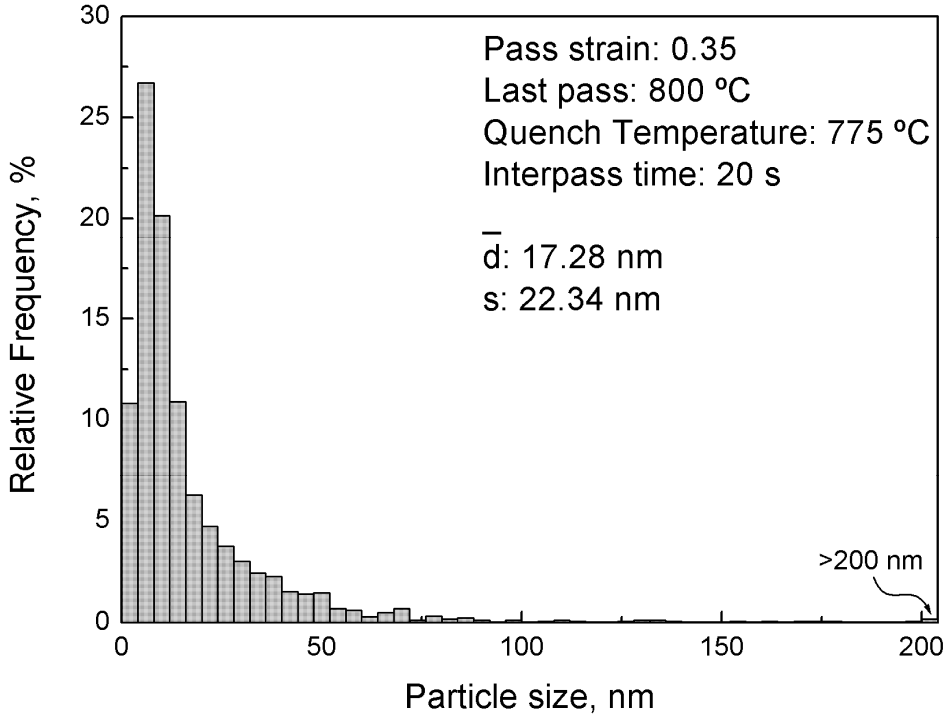
Pass strain: 0.35
Last pass: 800 ºC
Quench Temperature: 775 ºC
Interpass time: 20 s
d: 17.28 nm
s: 22.34 nm
>200 nm
Relative Frequency, %
Particle size, nm
0
5
10
15
20
25
30
0
50
100
150
200

b)

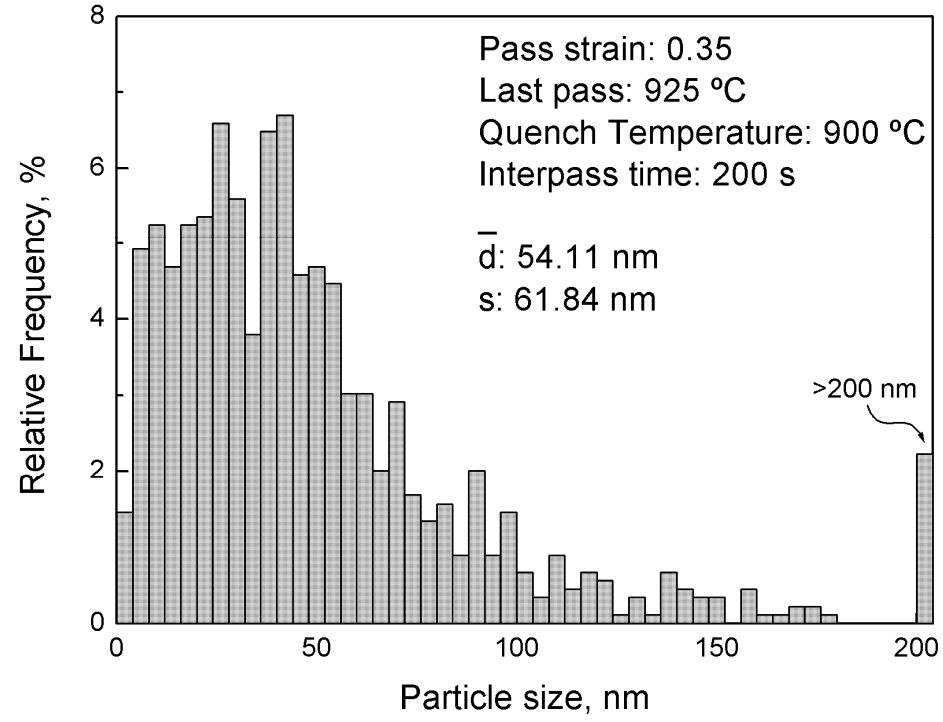

c)

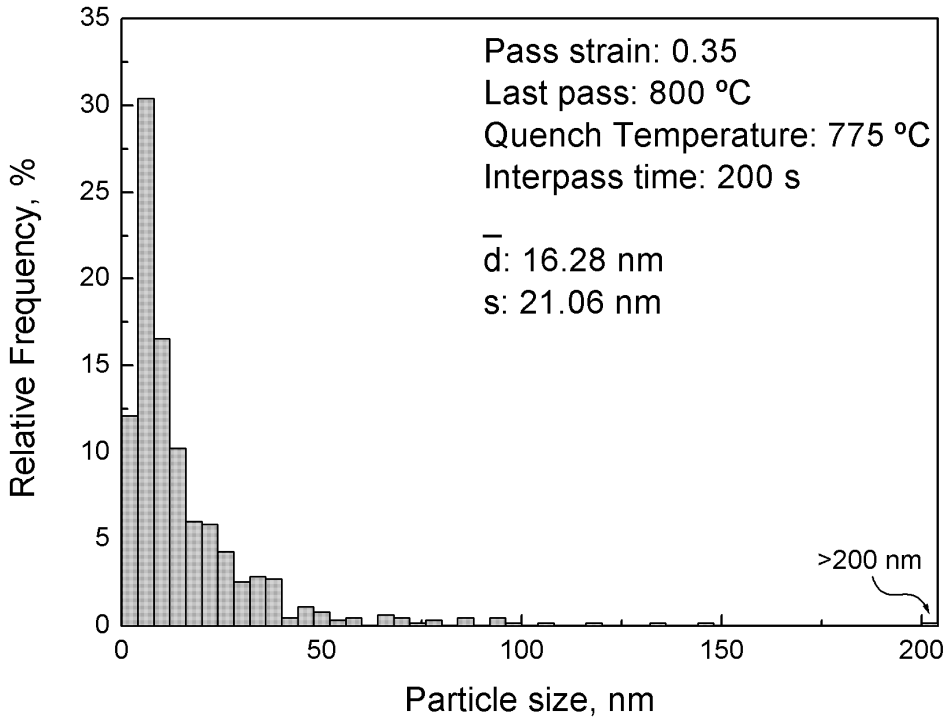

d)

Fig. 7. Precipitate size distributions obtained by hot rolling simulations in the following conditions: pass strain 0.35, pass strain rate 3.63 s^{-1}. **a)** Interpass time = 20 s, quenching at 900 ºC; **b)** Interpass time = 20 s, quenching at 775

ºC; **c)** Interpass time = 200 s, quenching at 900 ºC; **d)** Interpass time = 200 s, quenching at 775 ºC.

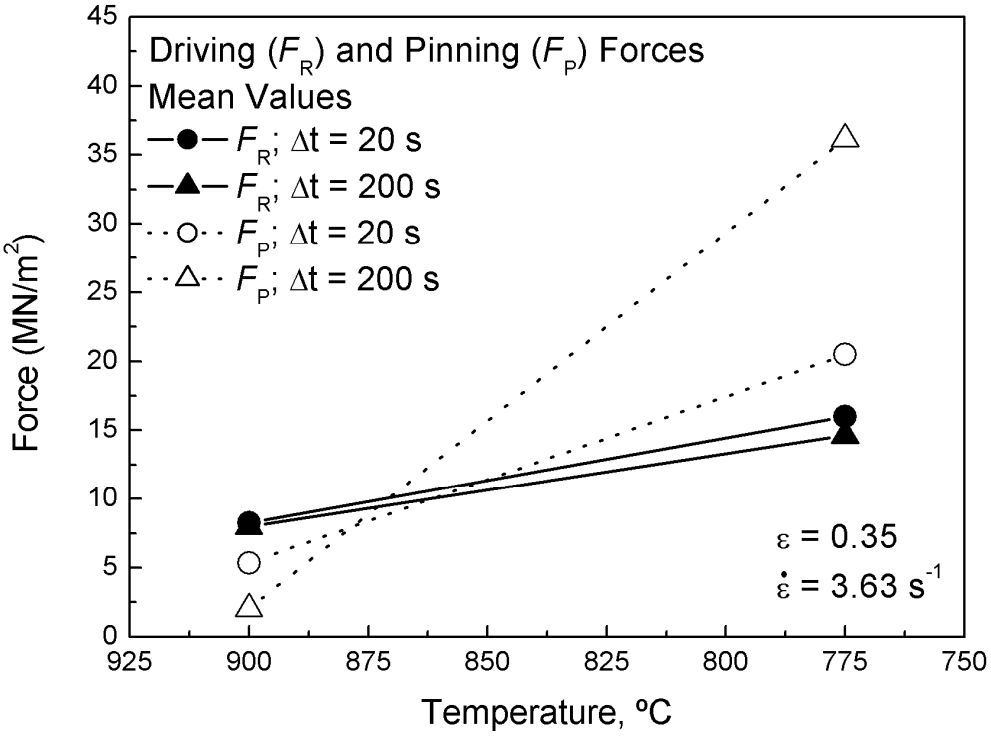

a)

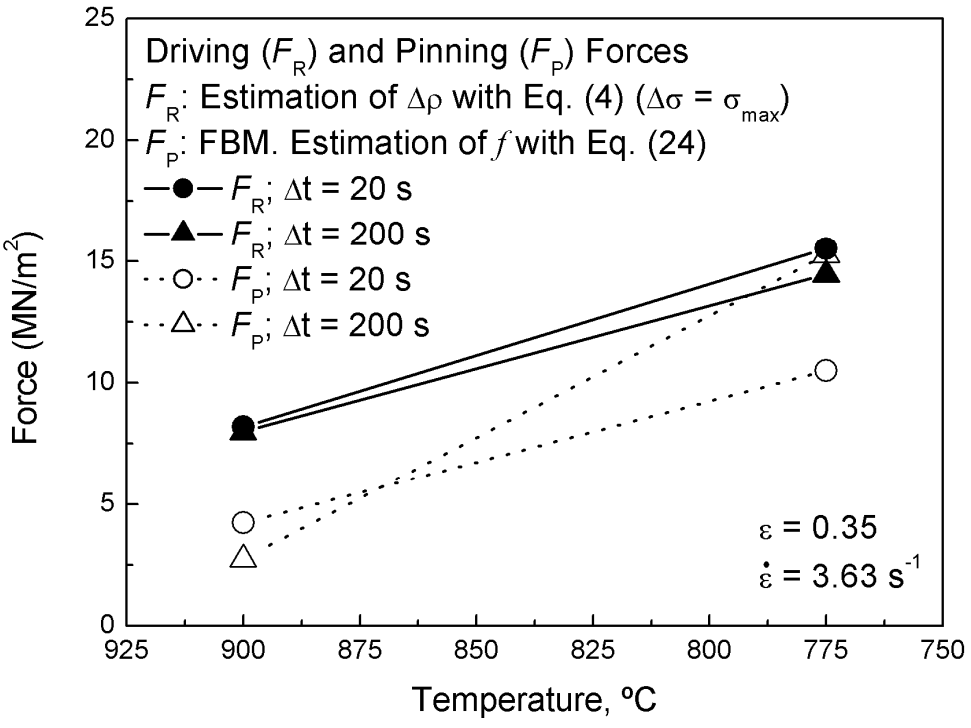

b)

Fig. 8. Estimation of recrystallization driving (F_R) and pinning forces (F_P) at 900 ºC and 775 ºC for the two studied hot rolling simulation schedules (Δt = 20 s and Δt = 200 s). **a)** Mean values of calculated F_R and F_P. **b)** F_R calculated after

estimation of dislocation density with Equation (4) assuming $\Delta\sigma$ = applied or maximum stress and F_P calculated following the FBM criterion and using TEM data to estimate the precipitated volume fraction *f*.